Simulations of clean drops rising into a layer of dissolved surfactant

David W. Martin,[1,*] Tamunotubo George,[2] and François Blanchette[2]
[1]*San Bernardino Valley College, 701 S Mt Vernon Ave, San Bernardino, California 92410, USA*
[2]*University of California, Merced, 5200 Lake Rd, Merced, California 95343, USA*

(Received 13 June 2018; published 8 January 2019)

We present simulations of clean drops rising into a layer of dissolved surfactant. Immediately after entering the surfactant layer, the drop is seen to accelerate suddenly as surfactant adsorbs onto its surface. The drop subsequently slows down to reach a terminal velocity that is between that of a clean drop and that of a solid object. For drops of viscosity equal to that of the ambient fluid, the terminal drop velocity, transition length, and maximal speed are all quantified and plotted against the Biot number, the ratio of convective to desorption timescales, and the adsorption number, the ratio of desorption to adsorption timescales. We find that faster sorption generally results in greater acceleration on entering the surfactant layer, a faster transition to equilibrium, and a faster terminal velocity. Drops of two different Reynolds numbers are considered to investigate the influence of inertial effects.

DOI: 10.1103/PhysRevFluids.4.014302

I. INTRODUCTION

When oil spills occur in the ocean, surfactants, also known as dispersants, are sprayed on the affected areas. This process is controversial, as it has the benefit of breaking up the oil into smaller droplets that are more easily absorbed by the ecosystem, but it can also increase the area over which oil spreads, and the dispersant themselves are highly toxic. It is thus important to be able to accurately predict the effects that surfactants may have on the dynamics of the oil spill.

When oil is released from the ocean floor, it will rise and breakup in drops. Whenever surfactants are used at the surface, the drops begin rising in surfactant-free water and eventually encounter water containing dissolved surfactants. Predicting the spread of the oil requires an accurate knowledge of its vertical speed, which is altered by its interactions with the dissolved surfactant.

Surfactants are substances whose molecules tend to reside on fluid-fluid interfaces. In most cases, they have hydrophobic and hydrophilic components, and minimize their potential energy when on the interface of water and another fluid. In that case, the surfactants' hydrophilic component can face the water, while their hydrophobic component faces away from the water. This, in turn, lowers the surface tension of the interface locally, which results in regions of lower or higher surface tension, depending on the surfactant concentration on the surface. Between these regions, Marangoni forces act to even out the surfactant concentration by spreading surfactants from regions of higher concentration to regions of lower concentration. All of these surface forces alter the rise speed of the droplets, and therefore the macroscopic dynamics of the system.

A considerable amount of research has been done on the effects of surfactants on the motion of buoyancy driven drops and bubbles. In the Stokes limit, the speed of buoyancy driven drops and bubbles was first calculated exactly in the absence of surfactants [1,2]. However, these results did not match subsequent experimental results [3–5], which found that the drops and bubbles moved more slowly than predicted, and in some cases, behaved like solid spheres. The physical basis

*Corresponding author: dwmath@gmail.com

for this discrepancy was explained by Frumkin and Levich [6] and was attributed to the presence of surfactants, which is very difficult to avoid experimentally. When surfactants are present, the flow on the outside of the drop drags the surfactant molecules toward the rear of the drop, where they accumulate. The resultant Marangoni forces act to counterbalance the increase of surfactant concentration at the rear, and so add to the drag on the drop, which lowers its rising speed. In regions of high surfactant concentration, stagnation, relative to the drop, was observed on the drop surface [5].

More recently, a number of numerical studies have quantified the effects of the degree of surfactant contamination [7], drop shape [8], and desorption rate [9]. A theoretical understanding of the dynamics has divided the parameter space into a number of different regimes. In terms of the degree of contamination, three regimes have been studied: clean (surfactant-free) or nearly clean drops, surfactant-laden drops with a stagnant or nearly stagnant cap, and a transition between the two [10,11]. Holbrook and Levan studied the nearly clean and nearly stagnant regimes asymptotically [12], and the intermediate region numerically [13]. Once the entire surface becomes stagnant, the drop behaves like a solid particle, and further increases of surfactant concentration will not change the speed of the drop, or the surrounding flow field.

The behavior of a surfactant-laden drop or bubble can also be categorized based on the relative importance of surface convection, bulk diffusion, and sorption rate. When bulk diffusion is slow, or the rate of sorption is small, compared to surface convection, sorption becomes negligible. If surface diffusion is also negligible, the drop surface becomes partitioned into two regions—a clean surface, toward the front of the drop, and a surfactant cap, toward the rear of the drop, where the flow field is stagnant [14–16]. In the limit of low Reynolds number, this so-called stagnant cap regime has been solved exactly [17,18].

When bulk diffusion and sorption occur on a similar timescale to surface convection, sorption effects cannot be ignored. In regions where bulk diffusion is slow but non-negligible, a boundary layer forms near the surface of the drop, in which the surfactant level rapidly decreases [10]. Early studies of sorption effects on drop velocity used a linear relation for both the sorption process and the relation between surfactant and surface tension [10,12,13]. Subsequent studies incorporate nonlinear sorption models and surfactant effects on surface tension, both for the Stokes limit [19,20], and at finite Reynolds number [21–23], including deformation [24–27] and transient effects [28].

We present here a numerical study of clean drops as they enter a surfactant layer. To the best of our knowledge, all existing studies of surfactant-laden drops consider drops that are already covered with surfactants. In addition to extending the parameter regimes previously studied in the long-term limit, we describe in detail the transition from surfactant-free to surfactant-laden, and the associated acceleration. We do so via an accurate and efficient numerical scheme that allows the exploration of the effects of changes in adsorption rate, desorption rate, and inertial effects. In Sec. II we formulate the problem–both the physical setup and the mathematical equations. In Secs. III and IV we present and validate, respectively, our numerical method for tracking sorption effects on a rising drop. In Sec. V we present the results of our simulations, and in Sec. VI we summarize and draw conclusions from those results.

II. SETUP AND GOVERNING EQUATIONS

We simulate a drop of radius R_0 rising along the central axis of a cylindrical container of radius $8R_0$ and height $32R_0$, as shown in Fig. 1. The drop begins at height $Z = 1.5R_0$ in a surfactant-free fluid. It rises and nearly reaches terminal velocity before, at a height of $10R_0$, entering a transition layer of thickness $0.1R_0$ where the surfactant concentration increases linearly. The drop then reaches a layer of constant surfactant concentration, $\Lambda = \Lambda_0$, where it continues to rise, eventually reaching steady state. The system is axially symmetric, and we only simulate the radial, R, and axial, Z, coordinates. We apply no-slip no-penetration boundary conditions to the walls of the cylinder but keep the walls far enough away from the drop that they only have a weak influence on the rising drop. Thus, our simulations model an infinite domain.

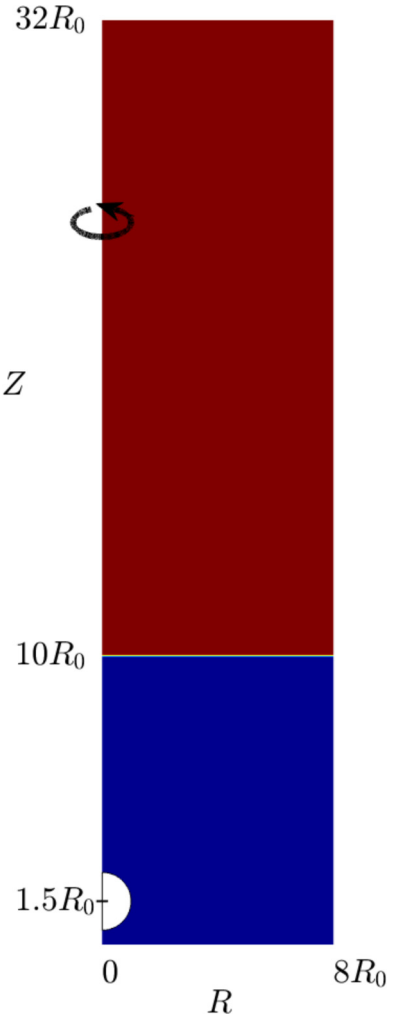

FIG. 1. The axially symmetric computational domain, with the axis on the left, and the wall on the right. The colors represent the concentration of dissolved surfactant: red for $\Lambda = \Lambda_0$ and blue for $\Lambda = 0$. The surfactant layer begins at $Z = 10R_0$.

We use the drop radius, R_0, as a length scale, and the drop density, ϱ_d, to scale the fluid density. We scale the fluid velocity using the Hadamard-Rybczynski speed, U_{HR}, given by

$$U_{\mathrm{HR}} = \frac{4g(\varrho_a - \varrho_d)R_0^2}{15\mu}. \tag{1}$$

The quantity U_{HR} represents the speed of a drop with density ϱ_d rising in an ambient of density ϱ_a under the influence of a gravitational acceleration, g, when the Reynolds number is zero, and no surfactant is present [1,2]. We assume for simplicity that the drop and ambient both have viscosity, μ.

The drop surface, $\mathbf{x}_s$, moves with the fluid and therefore obeys the equation

$$\frac{d\mathbf{x}_s}{dt} = \mathbf{u}|_{\mathbf{x}_s}, \tag{2}$$

where **u** is the fluid velocity. The fluid velocity satisfies the incompressible Navier-Stokes equations, which are, in dimensionless form:

$$\nabla \cdot \mathbf{u} = 0, \tag{3}$$

$$\rho \frac{\partial \mathbf{u}}{\partial t} + \rho \mathbf{u} \cdot \nabla \mathbf{u} = -\nabla p + \frac{1}{\mathrm{Re}} \nabla^2 \mathbf{u} + \frac{15}{4\mathrm{Re}} \phi \mathbf{k}, \tag{4}$$

where p is the dynamic pressure, obtained by subtracting the static pressure $p_s = -\rho_a g z$ from the true pressure, and Re is the Reynolds number, given by $\mathrm{Re} = \frac{\varrho_d R_0 U_{\mathrm{HR}}}{\mu}$, which quantifies the ratio of inertial to viscous forces. In Eq. (4), **k** is a unit vector in the positive vertical direction, and $\phi = \phi(r, z)$ is an indicator function that equals 1 inside the drop and 0 outside. The dimensionless fluid density, ρ, can be represented using the indicator function:

$$\rho(r, z) = (1 - \mathcal{D})\phi(r, z) + \mathcal{D} \quad \text{where} \quad \mathcal{D} = \frac{\varrho_a}{\varrho_d}. \tag{5}$$

We denote the dimensional surfactant concentration on the drop surface as Γ and that in the bulk fluid as Λ. The bulk exchange term, J, measures the net rate at which surfactants adsorb onto ($J > 0$) and desorb from ($J < 0$) the interface. It is given in dimensional form by the Langmuir-Hinshelwood kinetic equation [29,30]:

$$J(\Gamma, \Lambda|_s) = k_{\mathrm{ad}} \Lambda|_s \left(1 - \frac{\Gamma}{\Gamma_\infty}\right) - k_{\mathrm{de}} \Gamma, \tag{6}$$

where k_{ad} (with units m/s) and k_{de} (with units s^{-1}) are kinematic constants of adsorption and desorption, respectively, $\Lambda|_s$ is the bulk concentration evaluated on the drop surface (at $\mathbf{x}_s$), and Γ_∞ is the maximum packing concentration on the surface. We scale bulk surfactant concentration by its initial value, Λ_0, in the upper layer. An equilibrium surfactant concentration, Γ_0, can be obtained by setting $J = 0$ in Eq. (6). This results in the equation of state [29,30]:

$$\frac{\Gamma_0}{\Gamma_\infty} = \frac{\mathrm{Ad}}{1 + \mathrm{Ad}} \quad \text{where} \quad \mathrm{Ad} = \frac{k_{\mathrm{ad}} \Lambda_0}{k_{\mathrm{de}} \Gamma_\infty}. \tag{7}$$

The dimensionless quantity in Eq. (7) is the adsorption number, which measures the relative rate of adsorptive to desorptive processes. In natural and laboratory systems, the adsorption number is usually of order one. We note that the quantity Ad is inversely proportional to the maximum packing fraction, so reducing Ad can also be thought as increasing Γ_∞ for a fixed equilibrium concentration. Using these scales, we obtain a dimensionless exchange term

$$J(\gamma, \lambda|_s) = \mathrm{Bi}[\lambda|_s(1 + \mathrm{Ad} - \mathrm{Ad}\gamma) - \gamma], \tag{8}$$

where $\lambda = \Lambda/\Lambda_0$ and $\gamma = \Gamma/\Gamma_0$. The new dimensionless quantity appearing in Eq. (8) is a Biot number, given by

$$\mathrm{Bi} = \frac{R_0 k_{\mathrm{de}}}{U_{\mathrm{HR}}}, \tag{9}$$

which measures the desorption rate against the rising speed and the adsorption number.

We advance both the surface and bulk concentrations in time using advection-diffusion equations supplemented with surface-bulk exchanges [30]. They can be expressed in dimensionless form introducing Péclet numbers. On the drop surface we have

$$\frac{\partial \gamma}{\partial t} + \nabla_s \cdot (\gamma \mathbf{u}) = \frac{1}{\mathrm{Pe}_\Gamma} \nabla_s^2 \gamma + J(\gamma, \lambda|_s) \quad \text{where} \quad \mathrm{Pe}_\Gamma = \frac{U_{\mathrm{HR}} R_0}{k_\gamma}, \tag{10}$$

and the operator ∇_s is a gradient projected onto the drop surface. In the bulk we have

$$\frac{\partial \lambda}{\partial t} + \mathbf{u}\cdot\nabla\lambda = \frac{1}{\mathrm{Pe}_\Lambda}\nabla^2\lambda - \eta\delta_s J(\gamma, \lambda|_s), \quad \text{where} \quad \mathrm{Pe}_\Lambda = \frac{U_{\mathrm{HR}} R_0}{k_\lambda} \quad \text{and} \quad \eta = \frac{\Gamma_0}{R_0\Lambda_0}. \tag{11}$$

The constants k_γ and k_λ are diffusion coefficients on the drop surface and in the bulk, respectively. Here δ_s is a one-dimensional delta function located on the interface. The term $\delta_s \eta J(\gamma, \lambda|_s)$ captures the rate of surfactant exchanges between the interface and the bulk and effectively replaces a boundary condition on the normal derivative of λ. The number η represents the dimensionless thickness of a layer of bulk surfactant concentration that contains as much surfactant as the surface at equilibrium [31]. For simplicity, here we will set $\eta = 1$.

We relate the surface tension, σ, to the surfactant concentration using a linear elasticity equation [30,32], given in dimensionless form by

$$\sigma = 1 + \beta(1-\gamma). \tag{12}$$

The surface tension is normalized by the value, Σ_0, obtained at equilibrium in the surfactant layer, where $\gamma = 1$. The drop's surface tension when in the lower layer is therefore $\sigma = 1 + \beta$, and σ would approach one as $t \to \infty$, if the drop were stationary in the upper layer. The elasticity coefficient can be written as

$$\beta = -\frac{\partial \sigma}{\partial \gamma} = -\frac{\Gamma_0}{\Sigma_0}\frac{\partial \Sigma}{\partial \Gamma}. \tag{13}$$

Here, as is the case throughout the paper, the lowercase letters represent dimensionless quantities and the capital letters represent their respective dimensional quantities. The dimensionless version of Eq. (13) shows that β represents the rate at which surface tension decreases with increasing surfactant concentration. The dimensional version shows that β scales directly with the surfactant concentration, and inversely with the surface tension.

The surface tension affects the dynamics of the system through the stress boundary conditions, at the fluid-fluid interface [33]:

$$-\mathrm{Re}[p] + \mathbf{n}\cdot[\nabla\mathbf{u} + \nabla\mathbf{u}^T]\cdot\mathbf{n} = \frac{\mathrm{Re}}{\mathrm{We}}\sigma\kappa, \tag{14}$$

$$\mathbf{n}\cdot[\nabla\mathbf{u} + \nabla\mathbf{u}^T]\cdot\mathbf{t} = \frac{\mathrm{Re}}{\mathrm{We}}\frac{\partial\sigma}{\partial s} = -\mathrm{Mg}\frac{\partial\gamma}{\partial s}. \tag{15}$$

Here κ represents the total curvature (i.e., twice the mean curvature), $\mathbf{n}$ represents an outward unit normal to the drop surface, and $\mathbf{t}$ represents the unit tangent to the surface in the direction of increasing arc-length, s, measured from the bottom of the drop. Two new dimensionless numbers appear in Eqs. (14) and (15). The Marangoni number,

$$\mathrm{Mg} = \frac{\beta\mathrm{Re}}{\mathrm{We}} = \frac{\Sigma_0\beta}{\mu U_{\mathrm{HR}}}, \tag{16}$$

is a ratio of tangential surface stress to viscous stress and represents the importance of Marangoni effects relative to the viscous drag on the drop. We keep $\mathrm{Mg} = 2$ in all our simulations. The Weber number,

$$\mathrm{We} = \frac{\varrho_d R_0 U_{\mathrm{HR}}^2}{\Sigma_0}, \tag{17}$$

is a ratio of inertial to surface tension forces. In our setup, the Weber number represents how much the drop is likely to deform. We keep the Weber number small (see Table I), so that the drop remains approximately spherical. In the simulations we present, the drop aspect ratio varied by less than 2%.

In our simulations, rather than enforcing Eqs. (14) and (15) as boundary conditions, we include the surface stresses in the momentum equation using a delta function, δ_s, that is nonzero only on the

TABLE I. Parameter definitions and ranges in our simulations.

Parameter	Definition	Range
Re	$U_{\mathrm{HR}} R_0 \varrho_d / \mu$	1,20
We	$U_{\mathrm{HR}}^2 R_0 \varrho_d / \Sigma_0$	0.2
β	$-\partial\sigma/\partial\gamma$	0.02, 0.4
Mg	$\Sigma_0 \beta / \mu U_{\mathrm{HR}}$	2
$\mathcal{D}$	ϱ_a / ϱ_d	1.1
Pe_Λ	$U_{\mathrm{HR}} R_0 / k_\rho$	10^4
Pe_Γ	$U_{\mathrm{HR}} R_0 / k_\gamma$	100
Ad	$k_{\mathrm{ad}} \Lambda_0 / k_{\mathrm{de}} \Gamma_\infty$	0–16
Bi	$R_0 k_{\mathrm{de}} / U_{\mathrm{HR}}$	0.05–10
η	$\Gamma_0 / R_0 \Lambda_0$	1

interface [34–36]. Thus, for computational purposes, Eq. (4) becomes

$$\rho \frac{\partial \mathbf{u}}{\partial t} + \rho \mathbf{u} \cdot \nabla \mathbf{u} = -\nabla p + \frac{1}{\mathrm{Re}} \nabla^2 \mathbf{u} + \frac{15}{4\,\mathrm{Re}} \Delta\rho\phi \mathbf{k} + \delta_s \mathbf{F}_s, \tag{18}$$

where

$$\mathbf{F}_s = \frac{1}{\mathrm{We}} (\sigma\kappa \mathbf{n} + \nabla_s \sigma) = \frac{\sigma\kappa \mathbf{n}}{\mathrm{We}} - \frac{\mathrm{Mg}}{\mathrm{Re}} \frac{\partial\gamma}{\partial s} \mathbf{t}. \tag{19}$$

Because of the large number of dimensionless parameters in this system, we have summarized them in Table I. The range of values we consider for each parameter is presented in the rightmost column.

III. NUMERICAL METHOD

We solve Eqs. (3)–(18) using an approach described in more detail in Refs. [33,36]. Here, we briefly summarize the method used and provide a detailed description of the bulk-interface exchange term, which had not been previously presented. We use finite differences calculated on a staggered marker and cell (MAC) grid. A projection method [37] is used to compute a pressure that automatically enforces continuity. This gives rise to a Poisson equation for the pressure, which is inverted using iterative methods. We advance the solution in time using Euler's method and employ a volume of fluid (VOF) method [34] to track the fluid concentration, ϕ. The front is tracked using markers that are advanced in time according to Eq. (2). We relate the Lagrangian front to the Eulerian grid using bilinear interpolation. We interpolate between markers using cubic splines to obtain a smooth representation of the surface. The markers are redistributed at each time step to maintain a distance of $\sqrt{2}$ grid cells between markers. Each grid cell is a square of size $1/32$ drop radii. The pressure term is corrected to eliminate parasitic currents resulting from the pressure discontinuity at the interface [35]. This correction calculates a more accurate pressure gradient by taking into account the precise location of the interface and calculating the fraction of each cell on either side of the pressure discontinuity.

The surfactant concentration on the interface is tracked using a Lagrangian method that automatically conserves surfactant mass in the absence of sorption [33]. Before advancing the front, we compute the surfactant mass associated to each marker. After advancing the front, we correct the computed surfactant concentration to preserve mass over each curve segment between markers, and thus over the entire interface. Subsequently, we compute a surface diffusion term from finite differences on the markers, and a bulk-exchange term, which we discuss below.

Bulk surfactant concentration is advanced in time using Eq. (11) discretized at the centers of our MAC grid. The diffusive and advective terms are approximated with finite differences. Once

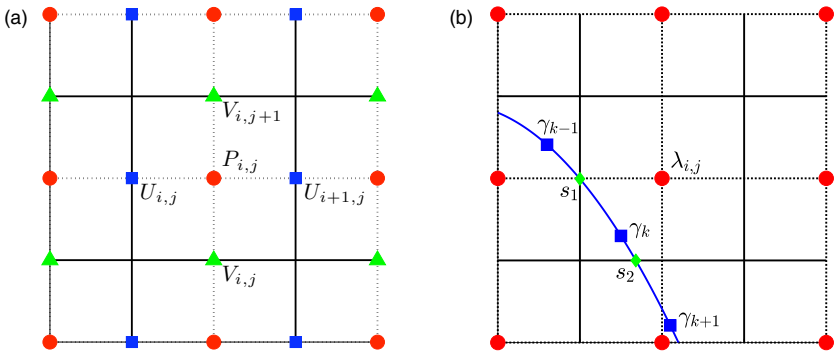

FIG. 2. Illustrations of the MAC grid used in our simulations. (a) Everywhere in the domain, the pressure, $P_{i,j}$, is stored at cell centers (red dots), and the horizontal (blue squares, $U_{i,j}$) and vertical (green triangles, $V_{i,j}$) velocities are stored on cell edges. (b) When an interface is present, surfactant concentration are also tracked. The dissolved surfactant concentrations, $\lambda_{i,j}$ are stored at cell centers everywhere (red dots), along with bulk sorption terms, $J_{i,j}$. The arc-lengths, s_k, surfactant concentrations on the surface, γ_k, and surface sorption terms, J_k, are stored at the markers (blue squares). The bounds of integration in Eq. (21) are located at the intersections of the cells and front (green diamonds).

the sorption term is added, the concentration is advanced in time using Euler's method. To prevent sorption from crossing the interface, we enforce a symmetry boundary condition at the fluid surface [33], using a discrete approximation, $\phi_{i,j}$, to the indicator function, ϕ, described in the previous section.

The two bulk-surface exchange terms are numerically very different. The surface concentration term that will be added to the kth marker, J_k, is accurately computed by evaluating a local line integral along the surface about each marker:

$$J_k = \frac{1}{s_{k+1/2} - s_{k-1/2}} \int_{s_{k-1/2}}^{s_{k+1/2}} J(\gamma, \lambda|_s)\, ds. \tag{20}$$

The changes in the surfactant concentration in the bulk, $J_{i,j}$, are added to the numerical cells intersecting the drop surface. They are computed by averaging over one grid cell. The delta function converts the area integral into a line integral along the surface:

$$J_{i,j} = \frac{1}{h^2} \iint_{\text{cell}_{i,j}} \eta \delta_s J(\gamma, \lambda|_s)\, dA = \frac{\eta}{h^2} \int_{s_1}^{s_2} J(\gamma, \lambda|_s)\, ds, \tag{21}$$

where h is the mesh width and s_1, s_2 are the locations (measured by arc-length along the interface) where the interface intersects the cell. The surface integrals in both of (20) and (21) are computed numerically using composite trapezoidal integration. The integrand, $J(\gamma, \lambda|_s)$, is given by Eq. (8), and depends only on arc-length. The surface concentration, $\gamma(s)$, is obtained by linear interpolation from the markers, and the bulk concentration, $\lambda|_s$, is obtained using bilinear interpolation from the adjacent cells. Figure 2 illustrates the role of the MAC grid in computing the surfactant concentrations.

IV. VALIDATION

Our simulations of drops rising in the presence of insoluble surfactants (no sorption term) have previously been shown to perform well in terms of conservation of drop mass, surfactant mass, and total energy of the system [33,36,38]. In particular, we found that variations in drop mass and total energy converged linearly with mesh width, h. In the simulations presented in Sec. V, $h = 1/32$, a resolution for which previous validations have shown that over the course of 38 000 time steps (approximately four dimensionless time units), drop mass varies by less than 0.1%, system

TABLE II. Percentage error in surfactant mass versus mesh width for a stationary drop undergoing desorption, at $t = 3$ with $\mathrm{Bi} = 1$. The error is measured as $(M_c - M_{th})/M_{th}$, where M_c is the surfactant mass obtained from the simulation, and M_{th} comes from Eq. (23).

	Percent error of	
Mesh width	M_γ	M_λ
$h = 1/8$	3.6×10^{-4}	0.0116
$h = 1/16$	1.2×10^{-4}	0.0040
$h = 1/32$	4.3×10^{-5}	0.0014
$h = 1/64$	1.5×10^{-5}	5.0×10^{-4}

energy varies by less than 1.6%, and surfactant mass is conserved up to round-off error. We have also validated our method by comparing it to a known theoretical solution in the simple case of a perturbed, irrotational drop [39]. For $h = 5/512$, computed oscillation frequency differed from the theoretical oscillation frequency by less than 0.33% [33,36]. Our method for advancing Eq. (11) in time has also been validated in the absence of sorption, and we found that the mass conservation of a stratifying agent showed better than second-order convergence [33]. For $h = 1/32$, the mass of the stratifying agent varied by about $1.93\times10^{-5}\%$ over approximately 20 units of dimensionless time.

We tested our computation of the surfactant exchange between the bulk and the surface in two ways: by computing an exact solution for a simple test case, and by measuring the conservation of total surfactant mass for a more strenuous test. Our simple test case involves a drop at rest in a stationary fluid that only undergoes desorption. In particular, we set $k_{ad} = 0$ in Eq. (6) and set the initial bulk concentration to zero. This gives, in nondimensional form,

$$J(\gamma, \lambda|_s) = -\mathrm{Bi}\gamma. \tag{22}$$

The drop is placed in the center of a cylindrical domain of radius and height equal to four drop radii, and remains stationary. We assume that the surfactant is initially uniformly distributed on the drop surface, $\gamma(s, t = 0) = 1$. Then the total surfactant mass on the surface and in the bulk at time t are given, respectively, by

$$M_\gamma(t) = 4\pi R_0^2 e^{-\mathrm{Bi}t} \quad \text{and} \quad M_\lambda(t) = 4\pi R_0^2(1 - e^{-\mathrm{Bi}t}). \tag{23}$$

We allowed surfactant to desorb from the surface until $t = 3$, with $\mathrm{Bi} = 1$, computed the total surfactant mass on the surface and in the bulk, and compared them against the values obtained from Eq. (23). The results, shown in Table II, demonstrate better than first-order accuracy.

We also tested the conservation of total surfactant mass for a deformed and oscillating drop, with $\mathrm{Bi} = 0.02$ and $\mathrm{Ad} = 10$. As before, the drop was placed in the center of a cylindrical domain with radius and height of four drop radii. In this case, we made our test more strenuous by introducing motion to the drop. In particular, we started the simulation with a spheroidal drop with aspect ratio $R_z/R_r = 1.5$ and allowed the system to relax over three units of dimensionless time. We started the simulation with no surfactant in the bulk and measured our error against the total initial surfactant mass. We found the error to be small, and to decay significantly with resolution, though the decay appears uneven for coarse resolutions (Table III). The change in bulk, surface, and total surfactant mass for a mesh width of $h = 1/32$ have also been plotted; see Fig. 3. Overall, we find that a resolution of $h = 1/32$ is sufficient to provide good conservation of all the quantities of interest, and we therefore use this resolution in the remainder of the paper. Simulations with large Bi or large Ad tended to have an increased resolution requirement and may therefore have a somewhat reduced accuracy.

TABLE III. Fractional change in surfactant mass versus mesh width for an oscillating drop undergoing sorption at $t = 3$ with $\mathrm{Bi} = 0.02$ and $\mathrm{Ad} = 10$. The variation is measured as $[M(3) - M(0)]/M(0)$, where $M(t)$ is the total computed surfactant mass of the system at time t.

Mesh width	Variation of M
$h = 1/8$	1.6×10^{-3}
$h = 1/16$	1.3×10^{-3}
$h = 1/32$	7.24×10^{-4}
$h = 1/64$	4.48×10^{-4}

V. RESULTS

We now present results obtained for a model of an oil drop rising to the surface of the ocean. In most oil spills, surfactants are sprayed at the surface, so our setup is that of a clean drop encountering a layer of surfactants of uniform bulk concentration. We elected to focus here on the case of drops of equal viscosity entering a sharp concentration jump, to emphasize the effects of the presence of surfactants. Another relevant setup to consider in the context of oil drops in the ocean would be that of a drop entering a surfactant concentration gradient. Although we focus here on drops with viscosity equal to that of the ambient water, realistic oil drops have a larger viscosity, which would dampen the effects seen for drops of equal viscosity. We begin our simulations with a drop at rest and allow it to accelerate to a steady rising speed before entering a layer where soluble surfactant is dissolved in the ambient fluid. The ambient surfactant concentration transitions sharply from a clean lower layer ($\lambda = 0$) to an upper layer of constant concentration ($\lambda = 1$), over the course of 0.1 drop radii. The transition is initially linear and takes place over the range $9.95 \leqslant z \leqslant 10.05$. For simplicity, we fix the Marangoni number at $\mathrm{Mg} = 2$. Bulk diffusion was kept as small as our simulations allowed, with $\mathrm{Pe}_\Lambda = 10^4$, which is comparable to the numerical diffusion in our simulations. The short-term effects of the dynamics of the bulk concentration boundary layer around the drop may therefore not be captured with great accuracy, but these are expected to be short-lived [40]. In addition, we could accurately capture the surface diffusion, assumed to be greater, $\mathrm{Pe}_\Gamma = 100$ and therefore likely to be dominant. In addition, we found that the observations reported here, such as the drop speed, varied by less than 1.5% when the resolution was doubled.

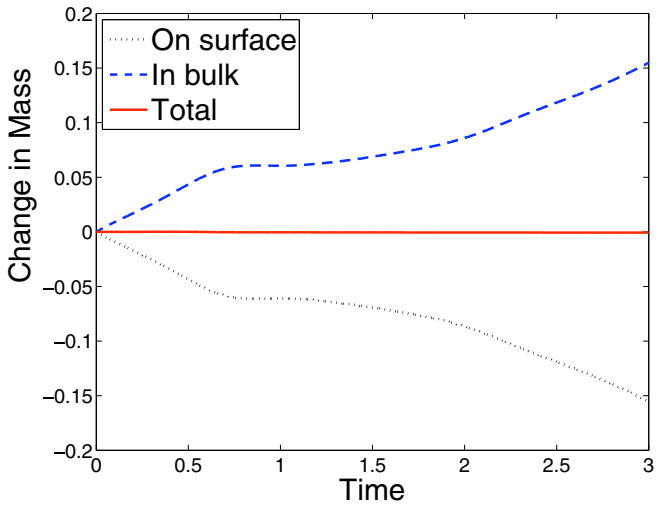

FIG. 3. Fractional change in surfactant mass over time for an oscillating drop undergoing sorption ($\mathrm{Bi} = 0.02$, $\mathrm{Ad} = 10$). The mesh width is $h = 1/32$.

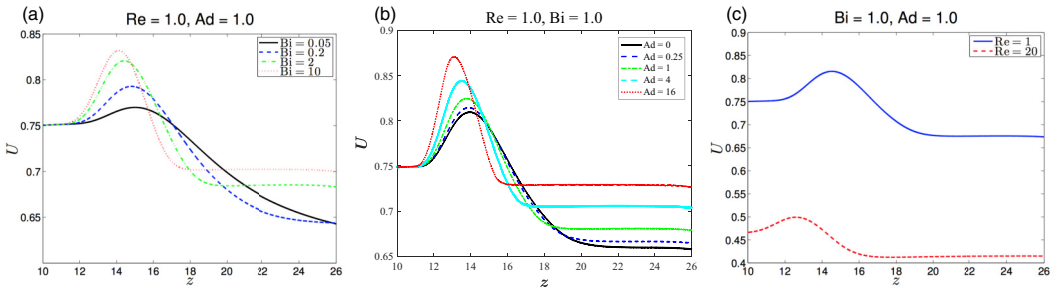

FIG. 4. The speed U of a clean drop as a function of height z as the drop enters a layer of soluble surfactant at $z = 10$. The reference value of the governing parameters are $\mathrm{Re} = 1$, $\mathrm{Ad} = 1$, and $\mathrm{Bi} = 1$, and in panel (a) we vary Bi, in panel (b) we vary Ad, and in panel (c) we vary Re.

A. Drop speed and concentration profiles

Figure 4 shows plots of the speed of the rising drop as it enters the surfactant layer. In all cases, the drop accelerates after entering the surfactant layer and subsequently decelerates to a steady ascent speed which is lower that the ascent speed in the lower layer. This is due to the surface tension gradient acting on the drop, as illustrated in Fig. 5(a) where the concentration profile along the drop surface is shown at different levels of the drop center. The top of the drop enters the bath first, adsorbing surfactant. The surfactant thus lowers the surface tension at the top of the drop relative to that of the bottom, resulting in a surface tension gradient that "sucks" the drop into the layer, in a manner similar to what is observed when a drop enters a layer where compositional differences reduce surface tension [41]. As the drop rises, convection carries surfactant toward the bottom of the drop, producing a gradient in the opposite direction that inhibits the rising of the drop. Eventually, the surfactant concentration reaches a steady-configuration with a higher concentration at the bottom, as seen in Fig. 5(a), which causes a surface tension gradient opposing the drop's rise, and results in a decreased steady-state speed.

As shown in Fig. 4(a), larger Biot number, corresponding to faster adsorption and desorption, results in a more vigorous suction, owing to the sharper surface tension gradient generated. The terminal speed also increases with an increased Biot number, because a high sorption rate tends to even out the surfactant concentration on the surface: higher concentrations of surfactant desorb faster, while lower concentrations adsorb faster. This results in weaker surface tension gradients opposing the drop motion, and thus rise speeds approaching those of a clean drop.

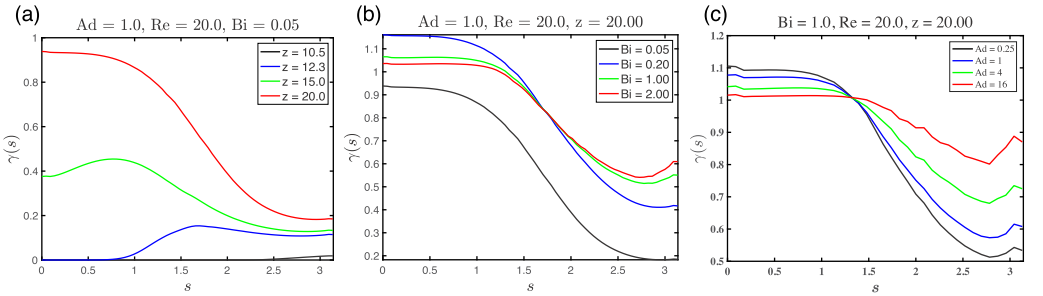

FIG. 5. Surfactant concentration as a function of arc-length along the drop's surface, starting from the bottom, where $s = 0$. Results are shown (a) as the center of the drop reaches various heights z, with $\mathrm{Ad} = 1$, $\mathrm{Re} = 20$, and $\mathrm{Bi} = 0.05$, (b) for various Biot numbers with $\mathrm{Ad} = 1$, $\mathrm{Re} = 20$, and $z = 20.0$, and (c) for various adsorption numbers with $\mathrm{Bi} = 1$, $\mathrm{Re} = 20$, and $z = 20$.

Figure 4(b) shows a similar dependence of speed profile on the adsorption number, a ratio of adsorption to desorption rates. After the initial acceleration, surfactants accumulate at the bottom of the drop, leading to Marangoni effects opposing the drop's rise. This effect is seen to be strongest for small Ad, as the concentration at the top of the drop remains low due to slow adsorption, and the concentration at the bottom approaches its equilibrium value. This results in large surface tension gradients opposing the drop's rise, and thus reduces both the peak and terminal speeds. For large values of Ad, the adsorption is nearly instantaneous, and the concentration gradient becomes weak. As the adsorption rate becomes large, the concentration of surfactants becomes nearly uniform, and the drop speed again approaches that of a clean drop. We note that the limit case $\mathrm{Ad} = 0$ is shown for completeness, but corresponds to the unrealistic situation where surfactants are not adsorbed, but have a nonzero concentration on the interface because the neighboring bulk concentration is nonzero, and thus still affect surface tension.

Similar speed profiles are obtained at $\mathrm{Re} = 1$ and $\mathrm{Re} = 20$, as shown in Fig. 4(c), though there are two key differences. First, the drop speed is overall lower at $\mathrm{Re} = 20$, which is a result of our nondimensionalization using the inertia-free drop speed. For the same drop size and mass, including inertial effect in general results in a slower rise speed. Second, we see that the suction effect is somewhat delayed at the low Reynolds number. This is somewhat counterintuitive, as one might anticipate that the drop's inertia would delay its response to changing forces. However, this effect is dominated by the amount of fluid entrained by the drop. In the more viscous regime, more fluid is entrained, which temporarily shields the drop from Marangoni effect, delaying the onset of the acceleration. For $\mathrm{Re} = 20$, less clean fluid is entrained by the drop and Marangoni effects are felt faster. For all the drops we considered, no substantial wake was observed, as streamlines did not detach significantly from the drop. Higher Reynolds numbers would likely yield a more pronounced wake that would have a potentially different effect on the drop, but this regime falls beyond the scope of the present study.

We see in Figs. 5(b) and 5(c) that similar surfactant concentration profiles are obtained when the rate of adsorption varies, through either the Biot or adsorption number, but that the magnitude of the concentration difference between the bottom and top of the drop decreases as adsorption takes place faster (larger values of Ad and Bi). In such cases, the system is able to reduce surface gradients through faster adsorption or desorption, leading to weaker Marangoni effects once the drop has fully transitioned into the upper layer.

B. Terminal velocity

The most extensively studied quantity in the long-term dynamics of the drop is its terminal velocity in the surfactant layer, away from the transition region. Denoting the terminal velocity as U_∞, we have quantified how it is affected by the adsorption rate, through both Bi and Ad. The normalized terminal velocity is shown in Fig. 6 as a function of the Biot number (a) and adsorption number (b) for two values of the Reynolds number. We ran simulations for Biot numbers as low as 0.02, but for the smallest Bi the terminal velocity was not reached within our computational domain and are therefore not included in Fig. 6. When adsorption is fast relative to convection, i.e., large Bi, the surface concentration gradients are nullified by the quick adsorption and the concentration of surfactant approaches its equilibrium value on the entire drop. We therefore expect that U_∞ will approach the speed of a clean drop as $\mathrm{Bi} \to \infty$, as has been reported by previous researchers [19]. On the other hand, as Bi approaches zero, adsorption becomes so slow that surfactants are effectively insoluble. In that case, U_∞ will approach the speed of a drop contaminated by insoluble surfactant [33], corresponding to approximately 0.8 when normalized by U_{clean}, (see column 4 of Table IV). Our results agree well qualitatively with previous results obtained for creeping flow [19], though a direct quantitative comparison is not possible as the parameters used do not match exactly. We note that the limit $\mathrm{Bi} \to 0$ does not correspond to a clean drop, as adsorption is still taking place, albeit slowly, and the terminal velocity then refers to the speed reached if time were also allowed to approach infinity. However, the distance required to reach that terminal velocity, as discussed below,

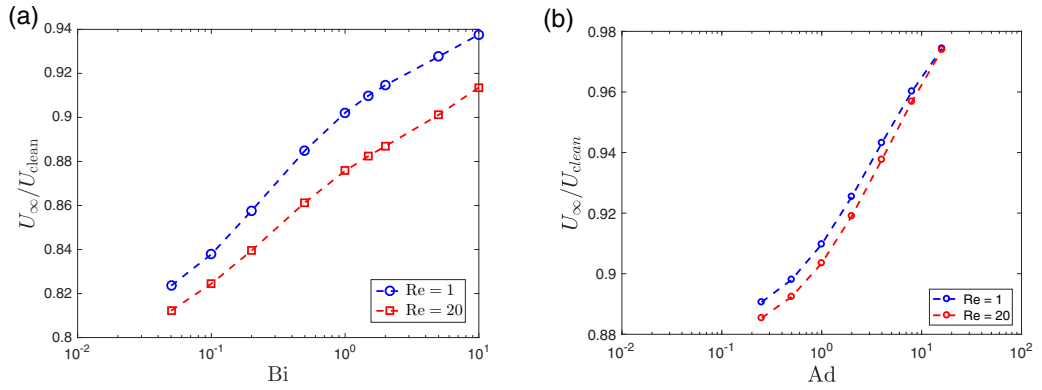

FIG. 6. Terminal velocity vs (a) Biot number and (b) adsorption number, for a drop rising in a surfactant layer, at two different Reynolds numbers. The terminal velocity is normalized by the steady-state speed of a clean drop for the same Reynolds number.

will increase indefinitely in that limit. The effects of the Biot number are also seen to be stronger at lower Reynolds number.

Figure 6(b) shows that increasing Ad results in a terminal velocity approaching that of a clean drop, similar to what is seen at large Bi, as Marangoni effects cannot be maintained when adsorption happens quickly. Our nondimensionalization is such that varying Bi or Ad corresponds to changing adsorption or desorption rates for a fixed equilibrium surfactant concentration. Increasing Ad therefore corresponds to increasing the adsorption rate relative to the desorption rate. As shown in Fig. 5, surface concentration gradients, and hence Marangoni effects, are greatest for small Ad, and consequently the terminal velocity is then reduced. Our approach emphasizes the effects of changing sorption rates but does not describe the effects of varying the potency of the surfactants (our Marangoni number was kept constant). Those effects have been described in previous studies [20], where the definition of the adsorption number includes the equilibrium concentration. In that notation, reducing the adsorption number also corresponds to reducing the equilibrium surfactant concentration, which leads to nonmonotonic effects as the surfactant potency changes together with its adsorption rate. Our results, especially for high Ad or Bi, fall into the so-called remobilization regime, in which the drop behaves more like a clean drop as Ad or Bi increases. If the equilibrium concentration is close to the maximum packing concentration, increasing Ad results in stagnation on the interface, and decreased drop speed, as was studied by previous authors [19,22]. This regime was not considered in the present study.

C. Transient effects

Two key elements may be used to describe the transition from the clean layer to the surfactant layer: the strength of the suction experienced by the drop upon entering the surfactant layer, and the

TABLE IV. Rising speeds for clean and insoluble surfactant-laden drops, obtained in a previous study [33]. For various Reynolds number, we give the rising speed of a clean drop relative to the Hadamard-Rybczynski speed (second column), a contaminated drop relative to the Hadamard-Rybczynski speed (third column), and a contaminated drop relative to a clean drop (fourth column).

Re	$U_{\rm clean}/U_{\rm HR}$	$U({\rm Mg}=2)/U_{\rm HR}$	$U({\rm Mg}=2)/U_{\rm clean}$
1	0.7486	0.6016	0.8036
10	0.5501	0.4438	0.8068
20	0.4723	0.3705	0.7845

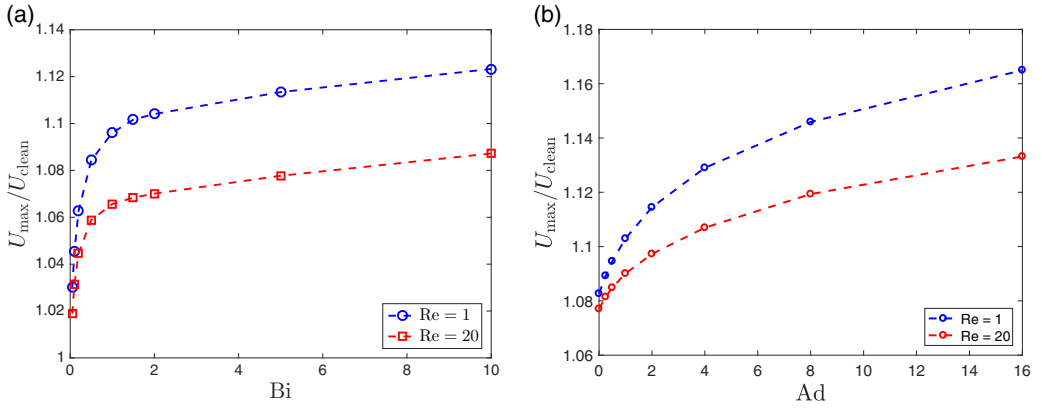

FIG. 7. Maximum speed attained as a clean drop enters a surfactant layer, normalized by the steady-state speed of a clean drop for the same Reynolds number. (a) The maximum speed's dependence on the Biot number, with Ad = 1 fixed; (b) its dependence on the adsorption number, with Bi = 1 fixed.

duration of its effect. We quantify the strength of the suction effect by the maximum speed reached, while the duration of the suction is measured by recording the distance over which its effects are felt. We note that preliminary results have shown that when the drop is more viscous than the ambient, as oil drops in the ocean would be, the suction effect is less vigorous, but the distance over which it is felt is larger.

Figure 7 shows the maximum speed reached, normalized by the steady-state speed of a clean drop, plotted against the Biot number in Fig. 7(a) and the adsorption number in Fig. 7(b). The results are given for Re = 1 and Re = 20 and show that the suction is slightly stronger at low Reynolds numbers. In the limit Bi $\to$ 0, we expect $U_{\max}$ to approach the terminal speed of a clean drop, as adsorption occurs infinitely slowly. As the Biot number increases, the rate of adsorption increases, and the acceleration of the drop is more vigorous. As Bi gets large, we expect the terminal speed to approach a maximal finite value, determined by a balance between convection and diffusion. Similarly, the dependence on Ad shows a stronger acceleration for larger adsorption numbers, though we anticipate this effect will level off as Ad is increased further.

To quantify the duration of the transition from the clean to the surfactant layer, we recorded the height, z_{trans}, at which the drop speed has come to within 1% of its terminal value in the upper layer. In Fig. 8 these transitional heights are plotted against the Biot number [Fig. 8(a)] and adsorption number [Fig. 8(b)]. The results are again given for Reynolds numbers of Re = 1 and Re = 20, emphasizing the longer delay due to entrainment at low Reynolds numbers. We expect that z_{trans} will go to infinity as Bi $\to$ 0 since this limit corresponds to adsorption being present but happening at a rate approaching zero. On the other hand, as Bi $\to \infty$, z_{trans} approaches a value of approximately six radii above the transition level, as the transition to equilibrium is determined entirely by convection. Increasing the adsorption number is also seen to reduce the extent of the transition region, though the effect of Ad is weaker. Notably, when inertial effects are increased, changing the rate of adsorption has only a minimal effect on the extent of the transition region. This is likely due to the reduced entrainment at higher values of Re, which results in adsorption taking place relatively quickly even for Ad $\sim$ 1.

D. Predicted profile

In all cases considered, we postulate that the vertical component of the surface tension gradient is the primary factor determining changes in the speed profile of the drop. This hypothesis can be tested by forming a predicted speed profile, based on the surface tension gradient alone:

$$U_{\text{pred}} = U|_{z=10} + a\overline{\nabla\sigma \cdot \mathbf{k}}, \tag{24}$$

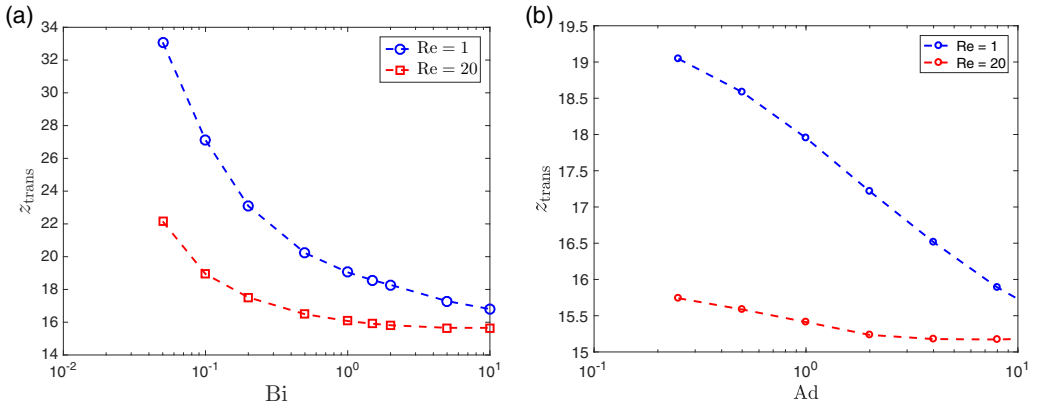

FIG. 8. Height, z_{trans}, at which the drop comes within 1% of its terminal speed vs the Biot number (a) and the adsorption number (b), at two different Reynolds numbers. The height is measured from the bottom of the cylindrical domain, and the surfactant layer begins at $z = 10$.

where $a > 0$ is a calibration parameter corresponding to a speed over drag ratio, per unit surface area. The quantity $\overline{\nabla\sigma \cdot \mathbf{k}}$ is the vertical component of the surface tension gradient, averaged over the surface of the drop, given by

$$\overline{\nabla\sigma \cdot \mathbf{k}} = \frac{1}{s_d}\int_0^{s_d} \frac{d\sigma}{ds}\sin\varphi\, ds, \tag{25}$$

where s_d is the total arc-length from the bottom to the top of the drop (generally, $s_d \approx \pi$), and φ is the angle to the vertical. Here Eq. (24) assumes that the forces acting on the drop are always at equilibrium, which is valid at low Reynolds numbers.

We computed $\overline{\nabla\sigma \cdot \mathbf{k}}$ by evaluating the right-hand side of Eq. (25) numerically. Figure 9 shows predicted and computed velocities versus height for given adsorption and Biot numbers for Reynolds numbers that are low, Re = 1, (a) and moderate, Re = 20, (b). Our prediction is highly accurate for a Reynolds number of Re = 1. The predicted speed is less accurate when Re = 20, where the most noticeable discrepancy is a lag in our predicted speed, or a delay in speed changes. This is consistent with inertial effects impacting the rise speed. In addition, the predicted speed is shifted vertically

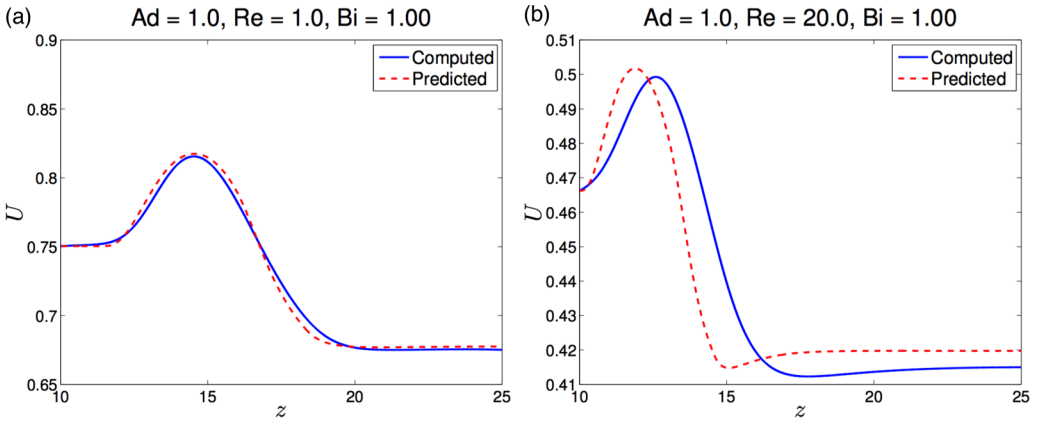

FIG. 9. For a clean drop entering a surfactant layer, computed speed vs a prediction based on surface tension gradients [see Eq. (24)], for Re = 1 (left), using a calibration parameter of $a = 1.34$, and Re = 20 (right), using a calibration parameter of $a = 16.76$. In both plots Ad = Bi = 1.

from the actual speed, which we suspect is due to the drop's own inertia. The results are similar for different Biot and adsorption numbers. A more detailed model could be developed based on Newton's second law by tracking the acceleration of the drop in terms of the instantaneous forces acting on the drop. However, capturing the dependence of the forces on the Reynolds number is beyond the scope of the present work, and we therefore limit our conclusions to stating that in the small Reynolds number regime, Eq. (24) yields an accurate prediction.

VI. SUMMARY AND CONCLUSION

We have applied a Volume-of-Fluid front tracking method to study rising surfactant-laden drops, examining a clean drop entering a surfactant layer. We have found that a drop rising at steady state into a layer of soluble surfactant undergoes changes in velocity based on the surfactant concentration gradient on the surface. As the drop first enters the surfactant layer, surfactant adsorbs onto the top of the drop, resulting in a surface tension gradient that quickly accelerates the drop. Past this transient stage, surfactant is advected by the flow and accumulates at the bottom of the drop, reversing the surface tension gradient and causing additional drag. At low Reynolds number, the drop velocity is nearly completely predicted by its instantaneous surfactant concentration distribution.

We have described the effects of the Biot and adsorption number on drops rising into a surfactant layer, as well as the effect of changing the Reynolds number from 1 to 20. Faster adsorption, corresponding to larger Biot and adsorption numbers, results in sharper surfactant concentration gradients during the suction phase, and milder gradients later on, increasing the rise velocity of the drop in both cases. Moreover, the duration of the transition is reduced when adsorption takes place faster, and when entrainment is reduced through an increase in inertial effects. In general, the terminal velocity of the rising drop is between that of a clean drop (Hadamard-Rybczinskii velocity in the absence of inertia) and that of a drop covered with insoluble surfactants which behaves as a solid ball (Stokes velocity in the absence of inertia). Faster sorption leads to behavior resembling that of a clean drop, as variations in surface tension are then quickly smoothed away. We anticipate that fast diffusive effects would have a similar effect. We found that our results for steady-state velocity are in good agreement with existing results for varying Biot numbers in creeping flow [19], and fall into the less studied [20] regime in which increasing the adsorption number increases drop speed. We note that the acceleration described here is similar to that experienced by drops entering a compositionally different layer where their surface tension becomes smaller [41]. In that case, the acceleration is even more pronounced, as compositional differences are effectively adsorbed instantaneously.

We focused in this study on characterizing the effects of adsorption. However, this system is very rich and complex, and other aspects of it therefore remain to be explored. Due to the large number of parameters at play, we held the Marangoni number and adsorption depth constant and considered only Reynolds numbers 1 and 20. However, real oil drops occur over a broad range of sizes and therefore of Reynolds numbers. We also restricted our attention to small Weber numbers, for which drops are only weakly deformed. Although work has been done on drop deformation at steady state [25], deformation effects upon entering a layer of dissolved surfactant remain to be investigated. The effects of the adsorption rate on the breakup of larger drops is an important consideration that remains to be investigated, as it determines the long-term size distribution of drops. We also kept diffusive effects small through large fixed values of the Péclet numbers. However, the presence of boundary layers depleted of surfactants around rising drops is known to influence their speed [10,40], and a study of their effects on transient motion remains to be undertaken. Also for simplicity, we used a linear surfactant relation throughout our study. For a more realistic physical picture, the effects of the Langmuir surfactant relation should be investigated for drops entering a surfactant layer, and perhaps even the full Frumkin relation, as has been done for steady-state motion [19]. Finally, we focused here on sharp transitions from clean to surfactant layers. In natural settings, the transitions are likely to be smoother, and considering a constant ambient surfactant concentration gradient would help provide a more complete picture of how oil drops rise in the oceans.

[1] J. S. Hadamard, Mouvement permanent lent d'une sphère liquide et visqueuse dans un liquide visqueux, C. R. Acad. Sci. **152**, 1735 (1911).
[2] W. Rybczynski, Über die fortschreitende Bewegung einer flüssigen Kugel in einem zahen Medium, Bull. Acad. Sci. Cracovie A40 (1911).
[3] F. H. Garner and A. H. P. Skelland, Some factors affecting droplet behaviour in liquid-liquid systems, Chem. Eng. Sci. **4**, 149 (1955).
[4] E. R. Elzinga and J. T. Banchero, Some observations on the mechanics of drops in liquid-liquid systems, Am. Inst. Chem. Eng. J. **7**, 394 (1961).
[5] T. J. Horton, T. R. Fritsch, and R. C. Kintner, Experimental determination of circulation velocities inside drops, Can. J. Chem. Eng. **43**, 143 (1965).
[6] A. Frumkin and V. Levich, On surfactants and interfacial motion, Zhur. Fiz. Khim. **21**, 1183 (1947).
[7] R. M. Edge and C. D. Grant, The motion of drops in water contaminated with a surface-active agent, Chem. Eng. Sci. **27**, 1709 (1972).
[8] T. Yamamoto and T. Ishii, Effect of surface active materials on the drag coefficients and shapes of single large gas bubbles, Chem. Eng. Sci. **42**, 1297 (1987).
[9] K. J. Stebe, S. Lin, and C. Maldarelli, Remobilizing surfactant retarded fluid particle interfaces. I. Stress-free conditions at the interfaces of micellar solutions of surfactants with fast sorption kinetics, Phys. Fluids A **3**, 3 (1991).
[10] D. A. Saville, The effects of interfacial tension gradients on the motion of drops and bubbles, Chem. Eng. J. **5**, 251 (1973).
[11] J. F. Harper, On spherical bubbles rising steadily in dilute surfactant solutions, Q. J. Mech. Appl. Math. **27**, 87 (1974).
[12] J. A. Holbrook and M. D. Levan, Retardation of droplet motion by surfactant. Part 1. Theoretical development and asymptotic solutions, Chem. Eng. Commun. **20**, 191 (1983).
[13] J. A. Holbrook and M. D. Levan, Retardation of droplet motion by surfactant. Part 2. Numerical solutions for exterior diffusion, surface diffusion, and adsorption kinetics, Chem. Eng. Commun. **20**, 273 (1983).
[14] P. Savic, *Circulation and Distortion of Liquid Drops Falling through a Viscous Medium* (National Research Council Canada, Ottawa, 1953).
[15] R. E. Davis and A. Acrivos, The influence of surfactants on the creeping motion of bubbles, Chem. Eng. Sci. **21**, 681 (1966).
[16] J. F. Harper, On bubbles with small immobile adsorbed films rising in liquids at low Reynolds numbers, J. Fluid Mech. **58**, 539 (1973).
[17] S. S. Sadhal and R. E. Johnson, Stokes flow past bubbles and drops partially coated with thin films. Part 1. Stagnant cap of surfactant film—Exact solution, J. Fluid Mech. **126**, 237 (1983).
[18] Z. He, C. Maldarelli, and Z. Dagan, The size of stagnant caps of bulk soluble surfactant on the interfaces of translating fluid droplets, J. Colloid Interface Sci. **146**, 442 (1991).
[19] J. Chen and K. J. Stebe, Marangoni retardation of the terminal velocity of a settling droplet: The role of surfactant physico-chemistry, J. Colloid Interface Sci. **178**, 144 (1996).
[20] Y. Wang, D. T. Papageorgiou, and C. Maldarelli, Increased mobility of a surfactant-retarded bubble at high bulk concentrations, J. Fluid Mech. **390**, 251 (1999).
[21] R. B. Fdhila and P. C. Duineveld, The effect of surfactant on the rise of a spherical bubble at high Reynolds and Péclet numbers, Phys. Fluids **8**, 310 (1996).
[22] R. Palaparthi, D. T. Papageorgiou, and C. Maldarelli, Theory and experiments on the stagnant cap regime in the motion of spherical surfactant-laden bubbles, J. Fluid Mech. **559**, 1 (2006).
[23] S. S. Dukhin, V. I. Kovalchuk, G. G. Gochev, M. Lotfi, M. Krzan, K. Malysa, and R. Miller, Dynamics of rear stagnant cap formation at the surface of spherical bubbles rising in surfactant solutions at large Reynolds numbers under conditions of small Marangoni number and slow sorption kinetics, Adv. Colloid Interface Sci. **222**, 260 (2015), Reinhard Miller, Honorary Issue.
[24] G. F. Andrews, R. Fike, and S. Wong, Bubble hydrodynamics and mass transfer at high Reynolds number and surfactant concentration, Chem. Eng. Sci. **43**, 1467 (1988).
[25] J. B. Mclaughlin, Numerical simulation of bubble motion in water, J. Colloid Interface Sci. **184**, 614 (1996).

[26] D. M. Leppinen, M. Renksizbulut, and R. J. Haywood, The effects of surfactants on droplet behavior at intermediate Reynolds-numbers. 1. The numerical-model and steady-state results, Chem. Eng. Sci. **51**, 479 (1996).
[27] S. S. Dukhin, M. Lotfi, V. I. Kovalchuk, D. Bastani, and R. Miller, Dynamics of rear stagnant cap formation at the surface of rising bubbles in surfactant solutions at large Reynolds and Marangoni numbers and for slow sorption kinetics, Colloids Surf. A **492**, 127 (2016).
[28] S. Tasoglu, U. Demirci, and M. Muradoglu, The effect of soluble surfactant on the transient motion of a buoyancy driven bubble, Phys. Fluids **20**, 040805 (2008).
[29] C. H. Chang and E. I. Franses, Modified Langmuir-Hinselwood kinetics for dynamic adsorption of surfactants at the air/water interface, Colloids Surf. **69**, 189 (1992).
[30] C. D. Eggleton and K. J. Stebe, An adsorption-desorption-controlled surfactant on a deforming droplet, J. Colloid Interface Sci. **208**, 68 (1998).
[31] C. H. Chang and E. I. Franses, Review. adsorption dynamics of surfactants at the air/water interface: A critical review of mathematical models, data, and mechanisms, Colloids Surf. A **100**, 1 (1995).
[32] H. A. Stone and L. G. Leal, The effects of surfactants on drop deformation and breakup, J. Fluid Mech. **220**, 161 (1990).
[33] D. W. Martin and F. Blanchette, Simulations of surfactant-laden drops rising in a density-stratified medium, Phys. Rev. Fluids **2**, 023602 (2017).
[34] B. Lafaurie, C. Nardone, R. Scardovelli, S. Zaleski, and G. Zanetti, Modelling merging and fragmentation in multiphase flows with surfer, J. Computat. Phys. **113**, 134 (1994).
[35] S. Popinet and S. Zaleski, A front tracking algorithm for the accurate representation of surface tension, Int. J. Numer. Meth. Fluids **30**, 775 (1999).
[36] D. W. Martin and F. Blanchette, Simulations of surfactant effects on the dynamics of coalescing drops and bubbles, Phys. Fluids **27**, 012103 (2015).
[37] D. L. Brown, R. Cortez, and M. L. Minion, Accurate projection methods for the incompressible Navier-Stokes equations, J. Computat. Phys. **168**, 464 (2001).
[38] F. Blanchette and Y. Lei, Energy considerations for multiphase fluids with variable density and surface tension, SIAM Rev. **51**, 423 (2009).
[39] J. C. Padrino, T. Funada, and D. D. Joseph, Purely irrotational theories for the viscous effects on the oscillations of drops and bubbles, Int. J. Multiphas. Flow **34**, 61 (2008).
[40] M. R. Booty and M. Siegel, A hybrid numerical method for interfacial fluid flow with soluble surfactant, J. Computat. Phys. **229**, 3864 (2010).
[41] F. Blanchette and A. M. Shapiro, Drops settling in sharp stratification with and without Marangoni effects, Phys. Fluids. **23**, 042104 (2012).